Total-Reflection Inelastic X-Ray Scattering from a 10-nm Thick La_{0.6}Sr_{0.4}CoO_{3} Thin Film

T. T. Fister, D. D. Fong, J. A. Eastman, H. Iddir, P. Zapol, P. H. Fuoss, M. Balasubramanian, R. A. Gordon, K. R. Balasubramaniam, and P. A. Salvador

Phys. Rev. Lett. **106**, 037401 — Published 18 January 2011

DOI: 10.1103/PhysRevLett.106.037401

Total reflection inelastic x-ray scattering from a 10 nm thick $La_{0.6}Sr_{0.4}CoO_3$ thin film

T.T. Fister,* D.D. Fong, J.A. Eastman, H. Iddir, P. Zapol, and P.H. Fuoss
Materials Science Division, Argonne National Laboratory

M. Balasubramanian
Advanced Photon Source, Argonne National Laboratory

R.A. Gordon
Department of Physics, Simon Fraser University,
Advanced Photon Source, Argonne National Laboratory

K.R. Balasubramaniam and P.A. Salvador
Materials Science and Engineering, Carnegie Mellon University

To study equilibrium changes in composition, valence, and electronic structure near the surface and into the bulk, we demonstrate the use of a new approach, total reflection inelastic x-ray scattering, as a sub-keV spectroscopy capable of depth profiling chemical changes in thin films with nanometer resolution. By comparing data acquired under total x-ray reflection and penetrating conditions, we are able to separate the O K-edge spectra from a 10 nm $La_{0.6}Sr_{0.4}CoO_3$ thin film from that of the underlying $SrTiO_3$ substrate. With a smaller wavelength probe than comparable soft x-ray absorption measurements, we also describe the ability to easily access dipole-forbidden final states, using the dramatic evolution of the La $N_{4,5}$-edge with momentum transfer as an example.

Surfaces and thin films in reaction environments (e.g. in solution or a high pressure gas) often have chemical and structural states that are significantly different from the material's bulk properties. Hard x-ray methods have a proven ability to probe surface, bulk, and interfacial material properties, often in extreme conditions such as chemical vapor deposition,[1], ultrahigh pressure,[2] or electrochemical potential.[3] However, the need for high-energy, penetrating x-rays precludes the study of first row elements and semicore excitations whose sub-keV binding energies typically require ultrahigh vacuum conditions. On the other hand, traditional direct methods of low energy core-shell excitations, such as x-ray absorption spectroscopy (XAS) and electron energy loss spectroscopy (EELS), are inherently surface sensitive due to the low mean free paths of the probe and the created photoelectron. Inelastic x-ray scattering (IXS) has increasingly been used as a bulk sensitive alternative to these techniques and was recently used to measure the surface phonon density of states by working at grazing incidence.[4, 5] Extending this approach to core-shell electronic excitations, we find that total reflection inelastic x-ray scattering (TRIXS) is capable of accessing dipole-forbidden states at high inelastic momentum transfers (q), unlike longer wavelength probes, like XAS, or forward scattering techniques like EELS.

While these effects should be generally applicable across a wide range of emerging material systems, we focus on an epitaxial, 10 nm-thick film of $La_{0.6}Sr_{0.4}CoO_3$ (LSCO) grown on $SrTiO_3$ (STO). By working at incident angles (α) above and below the critical angle for total reflection (α_c), we are able to isolate excitations only found in the film and substrate. Furthermore, the oxygen K-edge varies significantly between the coherently-strained film and underlying substrate, despite having similar crystal structures. Finally, we find that high-q TRIXS at the La $N_{4,5}$-edge gives rise to dipole-forbidden multiplet lines corresponding to lanthanum's unoccupied $4f$ states. The sensitivity of TRIXS to the chemical state of both cation and anion species could be a valuable tool toward understanding the oxygen reduction and exchange at the surface and interface of model oxide half cells at high temperature, variable gas conditions. These processes are widely considered to be the rate limiting steps in the performance of solid oxide fuel cells, where LSCO is often used as the cathode.[6]

We collected TRIXS at the lower energy resolution inelastic x-ray scattering (LERIX) endstation at the Advanced Photon Source[7]. LERIX is a multielement spectrometer that collects nineteen energy loss spectra simultaneously at momentum transfer q ranging from 0.8 - 10.1 $Å^{-1}$ at 10 keV. A schematic of the experiment for one analyzer/detector pair is shown in Fig. 1. Using the (555) silicon analyzer reflection (9890 eV), we measured 1.5 eV FWHM resolution from the quasielastic peak in grazing; this resolution is not significantly higher than the 1.35 eV resolution measured for the higher angle IXS since the scattering plane of each analyzer (seen in the inset of Fig 1) is orthogonal to the beam footprint. Despite losing 75% of the toroidally-focused incident flux to collimation (beam size was 500 × 50 μm at the sample), count-rates were still ≈200 cts/s at each analyzer at the height of the Compton background and 90 cts/s above the Compton background for the isolated oxygen

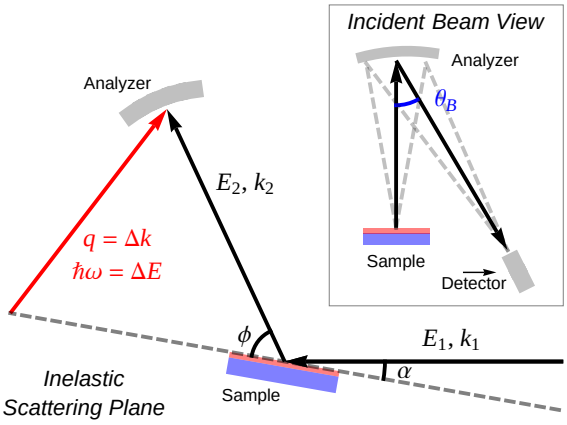

FIG. 1. The geometry of the incident and inelastically scattered x-rays is shown. The momentum transfer q is defined primarily by the angle between k_1 and k_2 while the energy loss is given by the monochromator energy E_1 and the analyzer energy E_2. The incident angle α can be used to tune the penetration depth. The inset depicts the Bragg scattering geometry of the sample analyzer and detector that defines E_2.

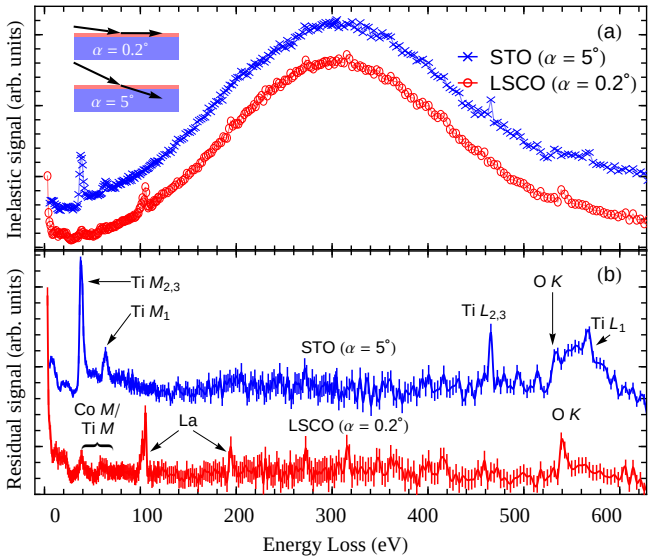

FIG. 2. (a) The IXS spectrum for q averaged over 8.3-9.5 Å^{-1} at $\alpha > \alpha_c$ and $\alpha < \alpha_c$, is shown. As demonstrated by the diagram in the upper left corner, the $\alpha = 5^\circ$ is bulk-sensitive since incident beam refracts 1 μm into the sample whereas the grazing $\alpha = 0.2^\circ$ spectrum only penetrates 5 nm. In each case, the broad, dispersive Compton profile (valence IXS), peaked at 300 eV, dominates the spectrum, while the fixed-energy core-shell features indicate the sensitivity to the substrate and film at angles above and below α_c. (b) To highlight the individual core-shell excitations, the same spectrum is replotted with the Compton scattering removed by a polynomial fit. The individual peaks are labeled and error bars based on Poisson statistics from the total IXS signal are given in the residual intensity. In both parts, the STO spectrum has been normalized and offset from the LSCO TRIXS data.

K-edge when integrated over all nineteen analyzers.

The LSCO film was grown on (001)-oriented $SrTiO_3$ using pulsed laser deposition at 750°C and 50 mTorr pO_2;[8] the film was later annealed at 700°C at 150 Torr pO_2 for one hour. Prior x-ray scattering measurements found that the film was coherently strained to the substrate lattice.

To confirm grazing incidence surface sensitivity, we measured wide-energy spectra well above, and well below the critical angle, α_c, for total reflection of the x-rays. As seen in Fig. 2a, the measured dynamic structure factor, $S(\vec{q},\omega)$, at high q is dominated by the Compton profile that results from valence electron IXS. When the energy loss is near an absorption threshold of a bound electron, there is a distinct jump in S due to the new scattering channel. The nonresonant core shell contribution to the overall IXS is

$$S_i(\vec{q},\omega) = \sum_f |\langle f|e^{i\ \vec{q}\cdot\vec{r}}|i\rangle|^2 \cdot \delta(E_2 - E_1 - \hbar\omega), \qquad (1)$$

where the energy terms and q are shown in Fig. 1, i is the initial state in the presence of the core-hole, f is the final state.[9] Note that in the low q dipole limit the expansion of the matrix element can be truncated at the linear term and $S_i(\vec{q},\omega)$ is proportional to the XAS signal $\mu(\hat{\epsilon},\omega)$, with the direction of q playing a similar role to the x-ray polarization $\hat{\epsilon}$. When $1/q$ approaches the length scale of the initial or final state wave function, quadratic and higher order terms in the expansion of $e^{i\vec{q}\cdot\vec{r}}$ begin to contribute to S_i, leading to new multipole selection rules that allow final states not accessible by standard spectroscopies.[9]

As shown in Fig. 2b, the positions of core-shell excitations contributing to the dynamic structure factor can be used to identify elemental species contributing to the IXS. At $\alpha = 5^\circ$, the substrate is expected to dominate the spectrum; for instance, the titanium lines are especially strong due to its large number of unoccupied d-states. At $\alpha = 0.2^\circ$, well below the critical angle for LSCO at 10 keV ($\alpha_c = 0.28^\circ$), the signal from the titanium is substantially suppressed, confirming total reflection of the x-rays. Additionally, signal from the lanthanum $N_{4,5}$ edge, that can only come from the 10-nm-thick LSCO film is immediately visible, due to the large number of unoccupied f-states.

To analyze the fine structure of the oxygen K-edge, which is present for both the film and substrate, we measured a finer energy scan that integrated over seventeen of the detector channels since the core-shell spectrum exhibited negligible q-dependence, as previously noted for similar measurements of the O K-edge in water ice.[10] Shown in Fig. 3a, the O K-edge from the LSCO film is noticeably different from the the bulk-sensitive STO spectrum; this chemical sensitivity is well-reproduced by an accompanying multiple scattering calculation[11] in

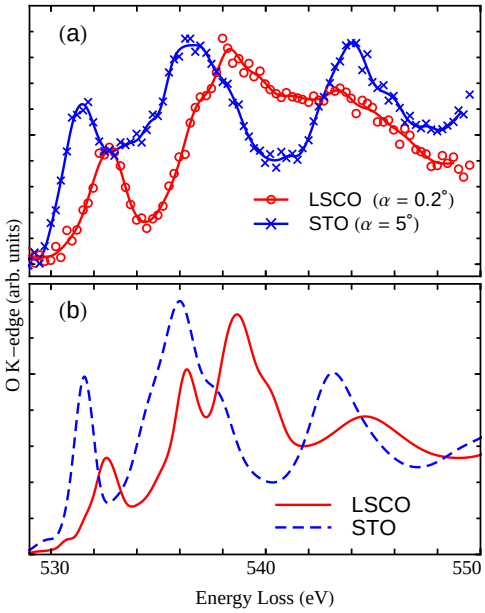

FIG. 3. (a) Normalized oxygen K-edge for LSCO and STO measured at $\alpha = 0.2$ and 5° respectively. Data have been averaged over all q. Splines through the data points are provided as a guide. (b) FEFF8.4 calculations for LSCO and STO spectra.

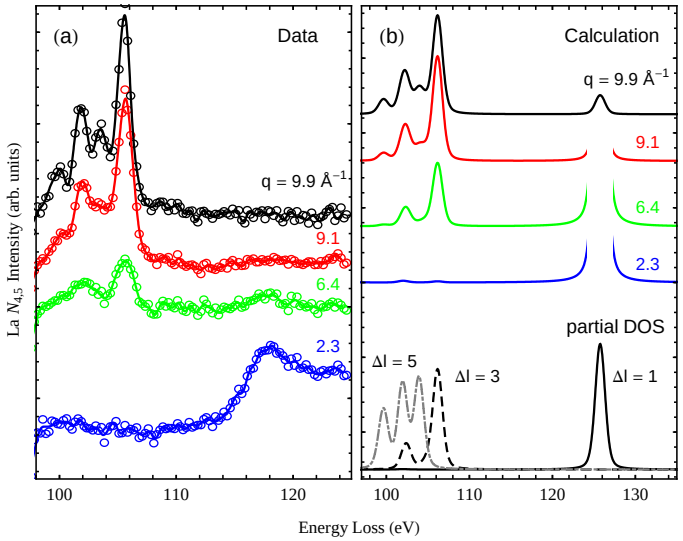

FIG. 4. (a) La $N_{4,5}$-edge contribution to measured IXS from LSCO ($\alpha = 0.25°$) as a function of q. Splines through the data points are provided as a guide. (b) Multiplet calculation for $4d^{10}f^0$ atomic states as a function of q (top) and the angular momentum components (bottom). The calculation, originally compared to Ce $4f^0$ data, [15], has been shifted by -9 eV to match the lower binding energy of the lanthanum edge. Data shown in (a) and (b) have been offset and scaled for comparison. Intensity from the calculated dipole resonance has been truncated to highlight higher order multiplets at intermediate q.

Fig. 3b. While there is no directly comparable experimental work to this composition and strain state of LSCO, we find that the O K-edge is very similar to prior EELS measurements.[12, 13]. Taking advantage of the *in situ* capabilities of TRIXS, changes in LSCO's oxygen stoichiometry (up to 8% of all oxygen sites at 1000°C[14]) are expected to be found in the integrated TRIXS intensity and near-edge structure at high temperature.

Unlike the O K-edge, the La $N_{4,5}$ spectrum exhibits considerable q-dependence resulting from dipole-forbidden multiplet states. This is in contrast to EELS, which is nearly always dipole-limited due to the q^{-4} prefactor in its double differential cross-section and the forward scattering geometry of a transmission electron microscope. Likewise, at low x-ray energies, XAS is limited to dipole transitions since the wavelength of the incident x-rays is much longer than the wavefunction of the initial state. By working with a short wavelength probe up to backscatter, TRIXS is capable of accessing states that are symmetry-forbidden by other low energy spectroscopies. As shown in Fig. 4a, one of the most dramatic examples of this new information are hybridized multiplet states in lanthanides. In LSCO, for example, the near-edge structure in the La $N_{4,5}$ edge largely consists of transitions from $4d^{10}f^0 \rightarrow 4d^9f^1$ states. For symmetry reasons, multiplet final states are restricted to $\Delta l = 1$, 3, and 5 transitions and are very sensitive to f-orbital occupation, oxidation state, and f-d hybridization.[15]

In the dipole approximation ($\Delta l = 1$), the La $N_{4,5}$-edge appears at 115 eV, leading to broad continuum states. While XAS and EELS are essentially limited to these states, TRIXS is capable of measuring sharp multiplet states at higher q. These atomic states, shown in Fig. 4a begin to appear near $q = 6.4$ Å^{-1} and evolve even further between 9 and 10 Å^{-1}. These states are due to the octupole ($\Delta l = 3$) and triakontadipole ($\Delta l = 5$) transitions arising from higher order terms in the expansion of $e^{i\vec{q}\cdot\vec{r}}$ in Eq. 1. To decouple final states by their angular momentum symmetry, it is convenient to expand the matrix element in Eq. 1 in a spherical harmonics basis.[16, 17] For cubic symmetry,

$$S(q,\omega) = \sum_f \sum_l |M_l(q,\omega)|^2 |\langle f|j_l(qr)|i\rangle|^2 \delta(E_i - E_f + \hbar\omega) \quad (2)$$

where $M_l = \sum_{m=-l}^{l} i^l 4\pi Y^*_{l,m}(\theta_q,\phi_q) Y_{l,m}(\theta_r,\phi_r)$ and j_l is a spherical Bessel function. For the theory shown in Fig. 4b, the initial and final states are approximated as Hartree-Fock wavefunctions.[18]. Using the appropriate weighting from $M_l(q)$, we see excellent agreement between this atomic theory and and the measured multiplets at high q. In general, the ability to easily access dipole-forbidden orbitals could be a valuable future tool for understanding f-electron occupation in lanthanide and actinide thin films.

In summary, we find that TRIXS is a powerful new spectroscopic tool for *in situ* measurements of the electronic structure near the surface and in the bulk of complex oxides, such as LSCO. Improved spatial depth resolution can be achieved using the α-dependence of the surface signal, similar to long period x-ray standing wave measurements that typically use x-ray fluorescence. Future studies will greatly benefit from additional x-ray focusing and better energy resolution. In addition to the unique $|q|$-dependence demonstrated above, changes in in-plane bonding and orbitals near the surface could also be further studied using the natural dichroism given by $\hat{q}$ for single crystal films.[19, 20] At lower energy losses (0-20 eV), this $\vec{q}$-dependence could also be valuable for studying the dipole forbidden $d-d$ excitations[21], color centers arising from surface defects, and the behavior of surface and bulk plasmons and excitons.[22]

We thank Maurits Haverkort and Josh Kas for assisting with the theoretical calculations and Gerald Seidler for reviewing the manuscript. The beamline staff at 20ID, Advanced Photon Source (APS) provided valuable assistance. Research at sector 20 is supported by the U.S. Department of Energy (DOE), NSERC, and its founding institutions. This research, including use of the APS, is funded by the DOE Basic Energy Sciences under contract DE-AC02-06CH11357 and by the DOE Solid-State Energy Conversion Alliance (TTF, KRB and PAS).

* fister@anl.gov

[1] A. Munkholm et al., Physical Review Letters **83**, 741 (1999).
[2] S. K. Lee, P. J. Eng, H. K. Mao, Y. Meng, and J. Shu, Physical Review Letters **98**, 105502 (2007).
[3] W. S. Yoon, C. P. Grey, M. Balasubramanian, X. Q. Yang, and J. McBreen, Chemistry of Materials **15**, 3161 (2003).
[4] B. M. Murphy et al., Physical Review Letters **95**, 256104 (2005).
[5] B. M. Murphy et al., Journal of Physics: Condensed Matter **20**, 224001 (6 pp.) (2008).
[6] F. S. Baumann, J. Fleig, H.-U. Habermaier, and J. Maier, Solid State Ionics **177**, 1071 (2006).
[7] T. T. Fister et al., Review of Scientific Instruments **77**, 063901 (2006).
[8] K. R. Balasubramaniam, S. Havelia, P. A. Salvador, H. Zheng, and J. F. Mitchell, Applied Physics Letters **91**, 232901 (2007).
[9] J. A. Soininen, A. Mattila, J. J. Rehr, S. Galambosi, and K. Hamalainen, Journal of Physics - Condensed Matter **18**, 7327 (2006).
[10] T. T. Fister et al., Physical Review B (Condensed Matter and Materials Physics) **79**, 174117 (2009).
[11] A. L. Ankudinov, B. Ravel, J. J. Rehr, and S. D. Conradson, Physical Review B **58**, 7565 (1998).
[12] I. Letofsky-Papst et al., Microscopy and Microanalysis **8**, 618 (2002).
[13] S. Stemmer, A. Sane, N. D. Browning, and T. J. Mazanec, Solid State Ionics **130**, 71 (2000).
[14] M. Sogaard, P. V. Hendriksen, M. Mogensen, F. W. Poulsen, and E. Skou, Solid State Ionics **177**, 3285 (2006).
[15] R. A. Gordon et al., EPL **81**, 26004 (2008).
[16] M. W. Haverkort, A. Tanaka, L. H. Tjeng, and G. A. Sawatzky, Physical Review Letters **99**, 257401 (2007).
[17] J. A. Soininen, A. L. Ankudinov, and J. J. Rehr, Physical Review B **72**, 045136 (2005).
[18] R. D. Cowan and D. C. Griffin, J. Opt. Soc. Am. **66**, 1010 (1976).
[19] A. Mattila et al., Physical Review Letters **94**, 247003 (2005).
[20] R. A. Gordon, M. W. Haverkort, S. S. Gupta, and G. A. Sawatzky, Journal of Physics: Conference Series **190**, 012047 (2009).
[21] B. C. Larson et al., Physical Review Letters **99**, 026401 (2007).
[22] P. Abbamonte et al., Proceedings of the National Acadamy of Sciences of the United States of America **105**, 12159 (2008).